NMR approaches to identify transient structure and interactions of intrinsically disordered dynein intermediate chain

Nikolaus M. Loening[1], Kayla A. Jara[2], and Elisar J. Barbar[2,*]

1. Department of Chemistry, Lewis & Clark College, Portland, Oregon, United States
2. Department of Biochemistry and Biophysics, Oregon State University, Corvallis, Oregon, United States

Corresponding author:

*Elisar J. Barbar
Elisar.barbar@oregonstate.edu

Abstract

Nuclear magnetic resonance (NMR) spectroscopy is widely recognized for its ability to provide atomic-level resolution of structures and interactions in intrinsically disordered proteins (IDPs). However, its application is often limited when studying large proteins that contain both structured and disordered regions. This challenge arises due to the broad peaks exhibited by structured regions in such proteins, which result from local compaction and restricted motions, complicating spectral analysis. Additionally, broadening in IDP complexes caused by exchange between free and bound states and/or the large size of the bound state, further obscures NMR signals and hinders the mapping of interaction sites. Moreover, IDPs are highly sensitive to proteolytic cleavage, necessitating careful handling and optimization during expression, purification, and data collection. In this study, we demonstrate how we successfully overcame these hurdles using examples from our work on the N-terminal region of the dynein intermediate chain (IC), which contains both α-helical and intrinsically disordered regions. By employing paramagnetic relaxation enhancement (PRE) NMR to probe conformational dynamics, water-amide chemical exchange to measure solvent accessibility, and saturation transfer difference (STD) NMR to map specific interactions with $p150^{Glued}$ and Nudel, we identified novel transient structures and interaction networks within IC. Our findings highlight the utility of these advanced NMR techniques in elucidating the dynamic behavior of IDPs and their complexes, providing valuable insights into their structural and functional roles.

Keywords

- NMR spectroscopy
- intrinsically disordered proteins
- dynein
- protein-protein interactions
- paramagnetic relaxation enhancement
- water-amide proton exchange

Introduction

Multiple essential processes, including those associated with signaling, cell division, and cellular differentiation, involve proteins which frequently contain intrinsically disordered regions. It is now well established that disordered regions regulate protein function through their high susceptibility to post-translational modifications, the frequency with which they are generated via alternative splicing, and the range of intra- and intermolecular interactions that they take part in that either promote or inhibit complex assembly [1–3]. Our work has focused on the cargo attachment subcomplex of the molecular motor dynein, a 1.6 MDa motor protein complex that uses the energy of ATP hydrolysis to translocate along microtubules to transport cellular organelles and various cargoes from the cell periphery to the nucleus [4]. Central to dynein's multiple functions is its interaction with the $p150^{Glued}$ subunit of dynactin via the intrinsically disordered N-terminal region of the dynein intermediate chain (IC) [5–7], which in mammalian systems is alternatively spliced and highly phosphorylated [8–10]. Dysregulation of dynein-dynactin interactions, for example, increases Golgi fragmentation, an early marker of neurodegenerative disorders [11]. Other partners for IC include the nuclear distribution protein (NudE) and its homolog Nudel (nuclear distribution protein NudE-like 1), which are implicated in neurodevelopmental and psychiatric disorders [12] and which bind at a site on IC that overlaps with the binding site on IC for $p150^{Glued}$ [13]. The disorder in IC has hindered resolution of its structure and interactions by cryo-electron microscopy and x-ray crystallography; thus, protein interactions in this part of the dynein complex remain unresolved in contrast to the extensive structural information available on the motor domain [14–16].

Solution-state nuclear magnetic resonance (NMR) spectroscopy has emerged as the method of choice for determining three-dimensional structures and interactions of small, dynamic, and soluble proteins. For structured proteins, nuclear Overhauser effect (NOE) enhancements are typically used to map through-space interactions that define the three-dimensional fold of proteins. This method, however, becomes limited for larger structured proteins as peaks disappear due to rapid transverse relaxation. In contrast, peaks for intrinsically disordered proteins (IDPs) remain sharp regardless of their length and the size of the protein, meaning they continue to be amenable to study by NMR [17–19]. Even with the extreme resonance overlap that is characteristic of disordered proteins, successful assignments for large proteins are prevalent in the literature [20–22]. However, resonance assignments are much more challenging for proteins that contain both structured and disordered regions. This is because such proteins tend to have large hydrodynamic radii (leading to slow overall tumbling) compared to folded/globular proteins with similar masses. Peaks for disordered regions sometimes remain sharp because local motion allows for line narrowing. In contrast, folded domains in such proteins suffer from being tethered at one or both ends to disordered regions, leading to long rotational correlation times and broad peaks which, in many cases, fully disappear. Examples of proteins with a mixture of structured and disordered regions where structural information is limited because only a fraction of assignments are observed for folded regions abound in the literature [7,23,24]. Furthermore, even with assignments in hand, structural information is limited because for highly dynamic disordered proteins, NOE enhancements will typically only appear between a nucleus and other nuclei in neighboring residues as longer-range interactions do not persist long enough to generate measurable NOE enhancements. In these situations, paramagnetic relaxation enhancements (PREs) can be used to observe long-range contacts and transient interactions [25,26].

Another challenge in the structural characterization of IDPs in complex with other proteins is that, in most cases, peaks disappear as components are titrated together to form complexes and

are too broad in fully-bound complexes to reappear. The common assumption is that peak disappearance takes place at the interfaces and thus we typically map sites of interactions to the peaks that disappear [6,27]. While this is often a reasonable assumption, there are other reasons why peaks can disappear. One reason is that folding in a region distant from binding can result in peak attenuation in that region, while another reason is that long-range contacts or transient interactions that are not necessarily at the interface can cause peak attenuation due to the formation of a more compact (and less dynamic) structure. Saturation transfer difference (STD) NMR is a powerful method for distinguishing between these possibilities [28,29], as STD will identify the binding epitope of a ligand when bound to its partner protein. Protons on the ligand that are at the interface receive a higher degree of saturation and, as a result, show stronger STD NMR signals, whereas protons that are either less involved or not involved in binding do not result in a signal in the STD NMR experiment, even if the peaks for these protons are attenuated in regular titration experiments.

In addition to PRE measurements and STD NMR, chemical exchange experiments that measure the exchange of amide protons with the solvent can identify amide protons that are more protected from the solvent in a disordered domain, and thus can be used to identify protection caused by transient structures [30,31]. By monitoring changes in the rate of water-amide chemical exchange upon titrating in a binding partner, it is possible to infer changes in transient interactions and structure caused by the binding interaction.

Previous work on dynein IC [6,32–35] has established that it contains an N-terminal α-helix (referred to as the single α-helix, SAH) followed by a disordered linker and a second helical region (H2). C-terminal of the H2 region is a long, disordered region that contains binding sites for dynein light chains. The α-helical propensity of the H2 region varies, ranging from only a nascent structure in fungi [33,35] and Drosophila [6], to being a fully-formed helix in mammalian constructs [34]. In the following, we use multidimensional NMR, PRE measurements, STD NMR, and chemical exchange measurements to more fully characterize the mammalian IC-2C isoform of dynein intermediate chain, and focus on the region of IC that interacts with $p150^{Glued}$ and Nudel. Using PRE measurements, we identify transient structures that were not observed by other relaxation measurements nor by secondary chemical shifts. Using a phosphomimetic mutant of IC-2C, we investigate the effect of phosphorylation on transient long-range interactions. Using STD NMR, we map direct binding of IC to its partners even when peaks for other regions not at the interface were attenuated. Our work shows that for large IDPs and their complexes it is important to leverage a combination of non-conventional NMR methods to gain insights into structure and function.

Methods

Protein Expression and Purification

Plasmids for generating recombinant *Rattus norvegicus* $p150_{382\text{-}531}$, $Nudel_{1\text{-}189}$, and IC-$2C_{1\text{-}96}$ were gifts (Erika Holzbauer, University of Pennsylvania). The sequences for $p150_{382\text{-}531}$ and $Nudel_{1\text{-}189}$ are 100% identical, and the sequence for IC-$2C_{1\text{-}96}$ is 94.8% identical, to the corresponding regions for *Homo sapiens*. All constructs have an N-terminal 6×His tag followed by a tobacco etch virus (TEV) cleavage site that leaves a four amino acid (GAHM) N-terminal cloning artifact after TEV protease cleavage to remove the 6×His tag. Single-cysteine mutants of IC-$2C_{1\text{-}96}$ (A9C, A44C, A62C, and A93C), as well as constructs with the S84D phosphomimetic mutation, were generated using site-directed mutagenesis.

^{15}N-labeled and unlabeled samples of proteins were expressed and purified as previously described [34]. Briefly, samples were grown either in Luria-Bertani media (for unlabeled samples) or ^{15}N-labeled MJ9 minimal media [36] at 37ºC until an optical density at 600 nm (OD_{600}) of 0.6 to 0.8 was reached. At this point, the cultures were induced by adding isopropyl-β-D-1-thiogalactopyranoside (IPTG) to a final concentration of 0.4 mM and were grown for another 3-4 hours. After pelleting the cultures by centrifugation, bacterial cell pellets were lysed by sonication and clarified by high-speed centrifugation. The clarified lysates were purified using immobilized metal affinity chromatography (IMAC) using a gradient of imidazole concentration varying from 20 to 500 mM. High-imidazole fractions containing the target protein were cleaved with His-tagged TEV protease [37] and simultaneously dialyzed overnight to reduce the imidazole concentration, after which the samples were purified again using IMAC. At this point, the target proteins appeared in the low-imidazole fractions whereas cleaved 6×His tag, His-tagged TEV protease, and metal-binding bacterial proteins were retained on the IMAC column. In most cases, the target protein was sufficiently pure for NMR spectroscopy at this point (>95% purity) but in some cases size-exclusion chromatography (SEC) was used as a final purification step. For samples containing cysteines, 2 mM dithiothreitol (DTT) was included in sample buffers.

For deuterated IC-2$C_{1\text{-}96}$, Rosetta(DE3) *Escherichia coli* cells (Merck KGaA, Darmstadt, Germany) transformed with plasmid for IC-2$C_{1\text{-}96}$ were grown in Luria broth prepared in 99.9% D_2O overnight. MJ9 minimal medium [36] prepared with 99.9% D_2O was inoculated using the overnight culture. ^{13}C and ^{15}N were supplied using uniformly-labeled [^{2}H,^{13}C] glucose (0.01 M) and [^{15}N] ammonium chloride (0.02 M), respectively. The cultures were grown to an OD_{600} of 0.8 and then induced with 0.4 mM IPTG at 26ºC. The resulting culture was then purified using the same procedures as for the unlabeled and ^{15}N-labeled samples.

Following purification, single-cysteine mutants of IC-2$C_{1\text{-}96}$ were labeled with the paramagnetic label *S*-(1-oxyl-2,2,5,5-tetramethyl-2,5-dihydro-1H-pyrrol-3-yl)methyl methanesulfonothioate (MTSL) using previously published protocols [38,39]. Briefly, samples were buffer exchanged using a desalting column into a labeling buffer (50 mM sodium chloride, 50 mM sodium phosphate buffer [pH 8]) and then reacted with MTSL in a 20:1 ratio (MTSL to target protein) for at least 2 hours in the dark at room temperature. Excess MTSL was then removed by desalting the samples into NMR buffer [50 mM sodium chloride, 10 mM sodium phosphate (pH 6.0)] after which they were concentrated.

Nuclear Magnetic Resonance (NMR) Spectroscopy

NMR spectra were collected using an Avance III HD 800 MHz spectrometer (Bruker BioSpin) with a TCI cryo-probe. Spectra for all IC-2C samples were taken at 15ºC in a buffer that contained 50 mM sodium chloride, 10 mM sodium phosphate (pH 6.0), 5% D_2O, and 0.2 mM DSS (sodium 3-(trimethylsilyl)propane-1-sulfonate).

PRE data were collected using 300 μM samples of ^{15}N/MTSL-labeled IC-2$C_{1\text{-}96}$ single-cysteine mutants using a BEST-TROSY-PRE experiment to measure proton transverse relaxation rates (^{1}H R_2) for the paramagnetic state of the sample and again after reducing the MTSL tag to a diamagnetic state by adding ascorbate to a final concentration of 4.3 mM. The BEST-TROSY-PRE experiment is a variant of the BEST-TROSY experiment [40] that includes an incremented delay time in the INEPT step [41]. This delay time results in a pseudo-dimension in which the degree of peak attenuation between different 2D planes can be fit to an exponential decay function to determine ^{1}H R_2. Eight delay times varying between 0 and 30 ms were used for the pseudo-

dimension, resulting in a total experiment time for each pseudo-3D BEST-TROSY-PRE experiments of approximately four hours.

HSQC-TROSY and (CLEANEX-PM)-TROSY experiments used 250 μM $^{2}H,^{15}N$-labeled IC-2C$_{1-96}$ and corresponding amounts of p150$_{382-531}$ and Nudel$_{1-189}$ (5–50 μM), whereas STD NMR experiments used sample concentrations of between 450 and 550 μM for $^{2}H,^{15}N$-labeled IC-2C$_{1-96}$ and 16–36 μM for p150$_{382-531}$ and Nudel$_{1-189}$. CLEANEX-PM spectra were acquired using a standard Bruker pulse sequence (trosycxf3gpphsi19) with a 0.5 W spin-lock pulse for the 100 ms mixing time and a total experiment time of approximately one hour. STD NMR experiments were acquired using a modified HSQC-TROSY pulse sequence (Bruker pulse sequence trosyetf3gpsi.2) with 2 s of 43 mW radiofrequency saturation at the beginning of the pulse sequence that alternated between being on-resonance with the methyl protons (0.9 ppm) and off-resonance (–40 ppm). The 2 s of saturation was implemented by repeating a 50 ms Gaussian shaped pulse 40 times. The receiver phase was alternated by 180º between scans with on-resonance saturation pulses and scans with off-resonance saturation pulses to generate the difference spectrum. The total experiment time for each STD NMR experiment was approximately six hours.

The data were processed using TopSpin 4.5.0 (Bruker BioSpin) and analyzed using CCPN Analysis 2.5.2 [42].

Results

PREs Identify Long-Range Contacts in IC Not Detected by Other Methods

Whereas the NOE arises from dipolar cross-relaxation between nuclei, PREs arise from dipolar interactions between unpaired electrons and nuclei, and result in increased relaxation rates for the nuclei [43]. In theory, any NMR-active nucleus can be used for measuring NOE enhancements as well as PREs, but the effect will be greatest for nuclei with the largest gyromagnetic ratio, so hydrogen nuclei (^{1}H) are most commonly used. For proteins, it is most common to measure PREs for amide protons due to the excellent signal dispersion found in ^{1}H-^{15}N correlation spectra.

Although both NOE enhancements and PREs have an r^{-6} dependence on the distance between the spins involved, the gyromagnetic ratio for an unpaired electron is some 660 times larger than that for ^{1}H so PREs are typically much more sensitive than NOE enhancements. In structured proteins, ^{1}H-^{1}H NOE enhancements can typically only be measured for distances up to ~6 Å, whereas PRE effects, at least in favorable cases, can be measured for distances up to ~35 Å. PREs are typically determined by measuring transverse relaxation rates (R_2), rather than longitudinal relaxation rates, as transverse relaxation is less influenced by internal motions and cross-relaxation. Consequently, in the following the difference in transverse relaxation rates (R_2) corresponding to when the sample is in a paramagnetic state and after the paramagnetic label has been reduced to a diamagnetic state was used to calculate the PRE (Γ_2) for a nucleus:

$$\Gamma_2 = R_{2,\text{paramagnetic}} - R_{2,\text{diamagnetic}} \quad (1)$$

Proteins that have one or more metal centers are good candidates for PRE measurements as the paramagnetic metal can be swapped with a diamagnetic metal (or vice versa) to measure the two relaxation rates that define the PRE. Proteins without metal centers are typically diamagnetic and, consequently, a paramagnetic center needs to be added by covalently attaching a paramagnetic spin label to the side chain of one or more of the residues [44]. This is most frequently done by attaching the relatively stable nitroxide radical *S*-(1-oxyl-2,2,5,5-tetramethyl-2,5-dihydro-1H-pyrrol-3-yl)methyl methanesulfonothioate (MTSL) to a cysteine sidechain [38]. As data analysis

is complicated by multiple spin labels in a protein, proteins used for PRE measurements are typically engineered to have only a single-cysteine residue.

Figure 1A shows PRE measurements for single-cysteine mutants of IC-2C$_{1-96}$ spin-labeled with MTSL. For residues in the sequence right next to the labeling site, the amide protons completely disappeared for the paramagnetic state so it was not possible to quantify the value of Γ_2. The extent to which residues close to the MTSL labeling site in the primary sequence were affected by the paramagnetic tag reflect the balance of structure versus disorder in that part of the protein. For example, when the spin label was in the SAH region (the A9C mutant), the rigid α-helical structure of this region resulted in a quick drop in Γ_2 values going toward the N- and C-termini. In contrast, when the MTSL label was located at residue 44 in the intrinsically disordered linker region (L1), a somewhat larger range of residues were affected as the lack of structure and presence of dynamics allowed more residues to come into close contact with the paramagnetic tag. When the spin label was located in the H2 region (the A62C mutant), a dip in Γ_2 values was observed around residue 50 due to the steric constraints of α-helical residues 52-62 preventing residue 50 from approaching the paramagnetic tag. The greater Γ_2 values observed around residue 45 are because these residues are far enough away along the flexible linker that they can approach the paramagnetic tag, as shown in the model in Figure 1B.

The addition of the MTSL label as well as the single-cysteine mutation could potentially influence the structure of IC-2C. However, in comparing ^{1}H-^{15}N correlation spectra of our MTSL-labeled single-cysteine mutants with spectra of wild-type IC-2C$_{1-96}$, we only observed changes in peak positions for residues in the immediate vicinity of the mutation site, and these changes rapidly diminished to the point of being indistinguishable from the wild-type chemical shifts for amides that are more than 2-3 residues away from the mutation site. These results indicate that there is no overall difference in the structure of the MTSL-labeled single-cysteine mutants relative to wild-type IC-2C$_{1-96}$; any changes are localized to the mutation site and are relatively subtle. Another caveat to interpreting PRE data is that the flexibility of the MTSL label can make quantitative work challenging [45,46]. However, in our case, we are using the PRE results qualitatively to establish which regions of IC-2C interact with each other, rather than to calculate distances or to generate a structural ensemble, so this is less of a concern.

PREs can also be used to test whether post-translational modifications change the structural ensemble for IDPs. For example, phosphorylation at serine 84 of IC-2C has been shown to block interactions with p150^{Glued} [47]. Based on studies with a phosphomimetic mutant (S84D) of IC-2C$_{1-96}$, we previously hypothesized that phosphorylation leads to a compaction of the structural ensemble that occludes the p150^{Glued} binding site on IC-2C [34]. However, Figure 1A shows that the PRE values from the double mutants (A9C/S84D, A44C/S84D, and A62C/S84D) were not significantly different from the PRE values for the corresponding single mutants, which contradicts this hypothesis. It is only in the case of the MTSL-labeled A93C mutant that we observed significant differences in the PRE values when the S84D mutation was included, and only for residues that were within ~10 residues of the MTSL label. This decrease in Γ_2 values for residues 80-95 of the L2 region in the A93C/S84D mutant indicates that this region spreads out (straightening the bend schematically shown at the end of the L2 region in Figure 1B/C), but otherwise the change in the electrostatics conferred by the S84D mutation does not alter interactions with other parts of IC-2C, as seen by the unperturbed small interaction with the SAH region. In addition, the lack of changes elsewhere in IC-2C$_{1-96}$ indicates that, in contrast to what we previously hypothesized [34], the overall structural ensemble does not become more compact.

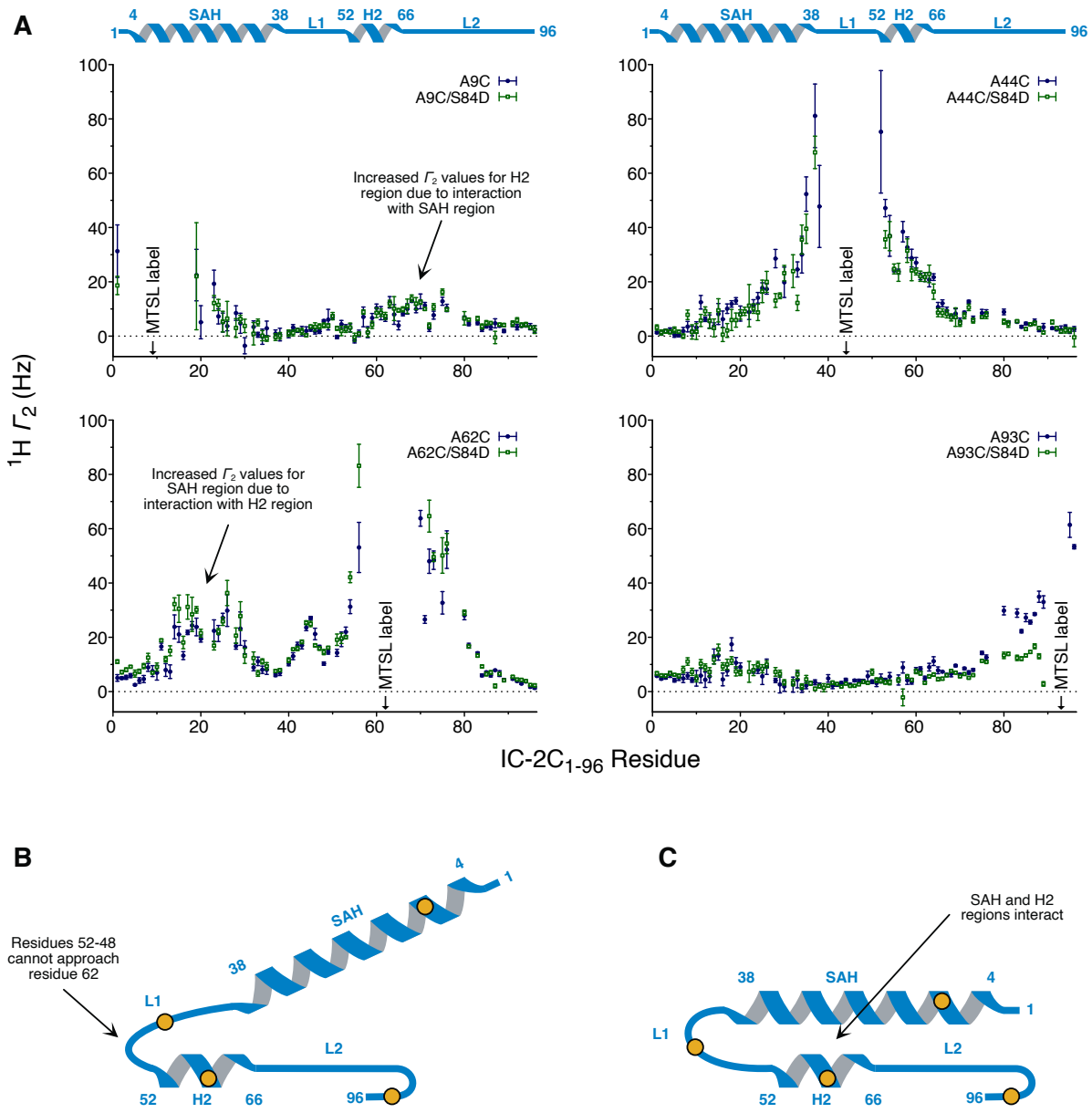

Figure 1. PRE measurements show compaction between the SAH and H2 regions of IC-2C$_{1\text{-}96}$ and that this interaction is not affected by a phosphomimetic mutation (S84D). (A) By using a series of single-cysteine mutants, the MTSL label could be positioned in the SAH (A9C), L1 (A44C), H2 (A62C), and L2 (A93C) regions of IC-2C$_{1\text{-}96}$. The increased PRE (Γ_2) values for the H2 region when the MTSL label is positioned in the SAH region (A9C), and for the SAH region when the H2 region is MTSL-labeled (A62C), shows that these regions of IC-2C interact. PRE measurements made using double mutants with a phosphomimetic mutation (S84D) show similar results, indicating that the phosphomimetic mutation does not induce long-range changes to the IC-2C$_{1\text{-}96}$ structural ensemble. **(B,C)** Schematic models of IC-2C$_{1\text{-}96}$ illustrate how residues 47-52 are sterically inhibited from approaching the MTSL label at residue 62 **(B)** and how a state in the structural ensemble that brings the SAH and H2 regions close to one another results in the increased Γ_2 values observed for the A9C and A62C mutants **(C)**. Orange circles represent approximate locations of the spin labels in the different single-cysteine mutant constructs.

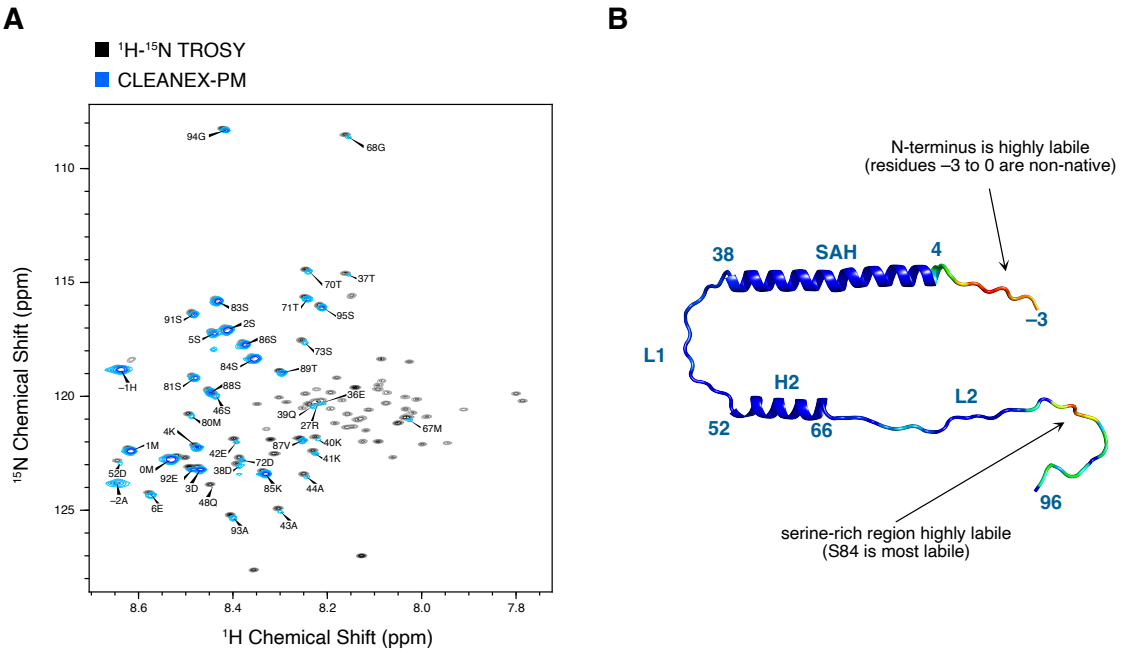

Figure 2. Water-amide proton exchange reveals areas of IC-2C$_{1\text{-}96}$ with varying degrees of protection from the solvent. (A) A ^{1}H-^{15}N HSQC-TROSY spectrum for IC-2C$_{1\text{-}96}$ (black) overlaid with the results from a (CLEANEX-PM)-TROSY experiment with a 100 ms mixing time (blue). Residues showing the greatest amount of exchange with the solvent are labeled. For clarity, the CLEANEX-PM spectrum is offset by 0.01 ppm in the ^{1}H dimension and by 0.1 ppm in the ^{15}N dimension. **(B)** CLEANEX-PM results mapped onto a model of IC-2C$_{1\text{-}96}$ generated using PyMOL [48]; red indicates amides that exchange the most with the solvent and dark blue indicates amides that exchange the least. The highest rates of exchange with the solvent are observed for N-terminal amides (residues –3 to 3), amides at the beginning of the SAH region (residues 4 to 6), and residues in the serine-rich part of the L2 region (residues 80 to 90).

Water-Amide Chemical Exchange Reveals Protected Local Structure

Using a TROSY version of the phase-modulated CLEAN chemical exchange (CLEANEX-PM) experiment [49,50], we observed which amide protons in IC-2C$_{1\text{-}96}$ readily exchange with solvent protons (Figure 2A). In the CLEANEX-PM experiment, signal is observed for magnetization that starts on H_2O and transfers to the amides via chemical exchange of the protons during the mixing time of the experiment. Although it is tempting to relate the lability with which amide protons exchange with the solvent to protein dynamics, this chemical exchange is the result of several processes in addition to local and global protein dynamics, including the degree of protection from the solvent by other parts of the protein (i.e., whether an amide is exposed to the surface of a protein or not), the stability with which protons are held in hydrogen bonds (such as between backbone amides and carbonyls in helices and sheets), and the degree to which water molecules are bound to the surface of a protein [51]. Consequently, the interpretation of water-amide proton exchange is not always straightforward, but exchange measurements can still provide insights into protein structure and dynamics when coupled with other sources of information.

As shown in the colored model for IC-2C$_{1-96}$ in Figure 2B, amide-water proton exchange is greatest for the N- and C-termini of IC-2C$_{1-96}$, as might be expected based on the dynamics of these regions previously determined using NMR relaxation measurements [34]. Also, as expected based on the strong hydrogen bonds that make up protein secondary structural elements, the amides in the α-helical SAH and H2 regions show no sign of exchange on the 100 ms time scale of our CLEANEX-PM experiment. Curiously, only low levels of exchange were observed for the L1 region as well as for the part of the L2 region near H2, despite their intrinsic disorder, indicating that there must be some sort of protection slowing down the rate of solvent exchange for these amides. This could possibly arise from transient interactions with other parts of the protein that protect these amides, but could also reflect local electrostatic effects. Most interestingly, exchange for the serine-rich part of the L2 region (residues 80-90) is higher than the C-terminus of the protein (residues 91-96). This is unexpected based on the previously published relaxation-based dynamics data [34], which show steadily increasing local motion for the IC-2C$_{1-96}$ construct going from the end of the H2 region to the C-terminus. We speculate that the high lability of the amide proton for S84, an important site for phosphorylation of IC [47], is related to the function of this protein.

Specific Mapping of Protein Interfaces

A great advantage of NMR spectroscopy compared to other structural biology techniques such as cryo-electron microscopy and x-ray crystallography is the ability to identify interactions between biomolecules in the solution-state in the absence of a three-dimensional structure, and the ease with which the properties of proteins can be probed by varying the temperature, titrating in acids or bases to vary pH, changing the ionic strength, adding binding partners, or even increasing pressure. For relatively small systems, binding interactions manifest as the appearance of new peaks, changes in peak heights, and/or shifts in peak position (chemical shift perturbations, CSPs), depending on the time-scale of the interaction. In addition, NMR-based measurements of NOE enhancements and chemical exchange can also provide insight into binding events.

Solution-state NMR is typically limited to systems with a total size less than ~20 kDa because larger systems tumble more slowly, leading to peak broadening that eventually becomes so severe that peaks are indistinguishable from the noise. Larger systems can become accessible by a combination of methodological advances, such as TROSY [52], deuteration [53,54], and focusing on methyl groups [55], but there are still greater challenges when studying such systems due to low sensitivity and the difficulty of assigning peaks.

One protein-protein interaction that we have been greatly interested in studying is the binding between the IC subunit of dynein and the p150^{Glued} subunit of dynactin [6,7,34,35,39,56]. A key difficulty with studying binding between constructs of the mammalian versions of IC (IC-2C$_{1-96}$) and p150^{Glued} (p150$_{382-531}$) is that the resulting 2:2 complex (492 residues, 56.8 kDa) is a challenging size to study by NMR, even when making use of TROSY and deuteration. The challenge is exacerbated by the coiled-coil structure of the p150$_{382-531}$ dimer [32], as the anisotropic tumbling of coiled-coils is especially unfavorable for the relaxation properties of amide protons [57,58]. As shown in Figure 3A, when ^{2}H,^{15}N-labeled IC-2C$_{1-96}$ is titrated with a substoichiometric amount of unlabeled p150$_{382-531}$, the amide peaks in ^{1}H-^{15}N HSQC-TROSY spectra for the IC-2C SAH region are greatly reduced in height and completely disappear by the time a stoichiometric binding ratio is reached and new peaks for the bound form never appear even at saturating concentrations. Also apparent in the data is a decrease in the peak heights for residues in the H2 region. Although these peaks do not completely disappear, the data are insufficient to unambiguously discern whether this is due to the H2 region weakly binding to p150^{Glued}, as has

been observed in *Chaetomium thermophilum* versions of these proteins [35], or whether this is only a consequence of a relayed effect from the interaction between the SAH and H2 regions. The disordered L2 region shows only modest decreases in peak heights as it is dynamic enough to experience motional averaging, even when a 1:1 ratio of the proteins is achieved. In contrast, the signals for the L1 region decrease despite its intrinsic disorder because its tethering to the structured SAH and H2 regions limits it motion in the bound complex, resulting in signal decreases that match those observed for the H2 region. The binding of IC-2C$_{1\text{-}96}$ with an N-terminal construct of another binding partner, Nudel [34,59], shows similar behavior (Figure 3B), with complete loss of signal for the SAH region of IC-2C$_{1\text{-}96}$ and partial signal loss for the H2 region. This construct (Nudel$_{1\text{-}189}$) forms a dimeric coiled-coil [13,60] so that it, like p150$_{382\text{-}531}$, is difficult to observe by NMR on its own or in complex with IC-2C$_{1\text{-}96}$ due to its relatively large size and because of its anisotropic tumbling.

The complete loss of signals for the SAH region when stoichiometric quantities of IC-2C$_{1\text{-}96}$ and p150$_{382\text{-}531}$ or Nudel$_{1\text{-}189}$ are combined necessitates indirect approaches to identify binding interfaces. One approach that uses the signal from the free state of a protein to probe the bound state is saturation transfer difference NMR (STD NMR) [28,29], which relies on applying radiofrequency irradiation to saturate signals of the large (and usually invisible) binding partner. This saturation is transferred to the smaller binding partner via spin diffusion while it is in the bound state, and results in a decrease in the signal of the free form of the smaller partner if the free and bound forms are in exchange on an appropriate time scale. Spectra with and without the saturation pulse are collected and subtracted from one another, resulting in a difference spectrum that highlights which nuclei are involved in binding.

In our case, we used a ^{1}H-^{15}N HSQC-TROSY version of the STD NMR experiment to observe how peak heights for IC-2C$_{1\text{-}96}$ amides changed upon saturating methyl protons for p150$_{382\text{-}531}$ or Nudel$_{1\text{-}189}$. For STD NMR to work, it is necessary to saturate methyl protons of the binding partner without affecting IC-2C$_{1\text{-}96}$, which we accomplished by using a ^{2}H,^{15}N-labeled IC-2C$_{1\text{-}96}$ sample in which aliphatic groups are deuterated but amides are still protonated due to exchange with the solvent. In theory, a control STD NMR spectrum of IC-2C$_{1\text{-}96}$ on its own should have no peaks but, in practice, there will always be weak STD peaks as shown in Figure 4A. This is because deuteration is never perfect so a small fraction of the IC-2C$_{1\text{-}96}$ methyl groups will still be protonated and therefore will become saturated and transfer this saturation to amide protons. Unsurprisingly, most of these weak STD peaks are for residues with methyl groups or residues that are adjacent to methyl-containing residues.

When a substoichiometric amount of p150$_{382\text{-}531}$ is titrated into the ^{2}H,^{15}N-labeled IC-2C$_{1\text{-}96}$ sample, large increases in the STD signal for IC-2C$_{1\text{-}96}$ are observed for amides in the SAH region (Figures 3C and 4A). Not only does this confirm that the SAH region of IC-2C binds to p150^{Glued} (as was apparent from the decrease in peak heights for the entire region observed in Figure 3A), but it also shows an additional detail that only a subset of the SAH residues (residues 7-21) make close contacts with p150$_{382\text{-}531}$. In addition, the lack of changes in the STD peak heights for the H2 region answers the question posed by the data in Figure 3A as to the mechanism underlying the decrease in peak heights for the H2 region. The unaltered STD signals for this region upon adding p150$_{382\text{-}531}$ means that there is no direct interaction between the H2 region and p150$_{382\text{-}531}$. Rather, the peak height decreases observed in the HSQC-TROSY spectra must be due to the SAH/H2 interaction increasing the correlation time for the H2 region when the SAH region binds to p150$_{382\text{-}531}$. Further increasing the amount of p150$_{382\text{-}531}$ in the sample (30:1 IC-2C$_{1\text{-}96}$:p150$_{382\text{-}531}$)

results in larger STD signals for residues 7-21 of IC-2C, which demonstrates that the STD effect is concentration-dependent, as would be expected for protein-protein binding.

The STD signal when $Nudel_{1\text{-}189}$ is titrated into the sample shows similar behavior (Figures 3D and 4A). As is observed when titrating in $p150_{382\text{-}531}$, the lack of an STD signal for the H2 region demonstrates that the H2 region does not directly interact with the binding partner. In addition, we can see that $Nudel_{1\text{-}189}$ interacts with the same binding site along IC-2C (residues 7-21), in agreement with previous work showing that these proteins bind dynein intermediate chain competitively [13,61].

By subtracting the constant STD signals seen in the control sample from the STD signals when $p150_{382\text{-}531}$ or $Nudel_{1\text{-}189}$ are present it is possible to better visualize the increase in signal for $IC\text{-}2C_{1\text{-}96}$ due to interactions with the binding partner. Plotting the resulting double difference values for binding with $p150_{382\text{-}531}$ (Figure 4B) or with $Nudel_{1\text{-}189}$ (Figure 4C) onto models of $IC\text{-}2C_{1\text{-}96}$ helps illustrate the localization of the protein-protein interaction to the N-terminal end of the IC-2C SAH region.

Exchange between amide and solvent protons can also be used to provide insights into changes in local structure and solvent protection upon binding. The exchange between solvent and amide protons for $IC\text{-}2C_{1\text{-}96}$ shown in Figure 2 changes upon adding $p150_{382\text{-}531}$ (Figure 3E) or $Nudel_{1\text{-}189}$ (Figure 3F). In both cases we find a decrease in the amount of exchange for residues at the N-terminus, indicating that this end of the SAH region either becomes more structured upon binding or is shielded from the solvent by the binding partners. In contrast, the amide protons in the L2 region are unaffected by binding and maintain the same amount of exchange with the solvent. A small decrease in the amount of exchange is also observed for the L1 region, most likely reflecting a degree of shielding and a slowing of dynamics for this region upon binding.

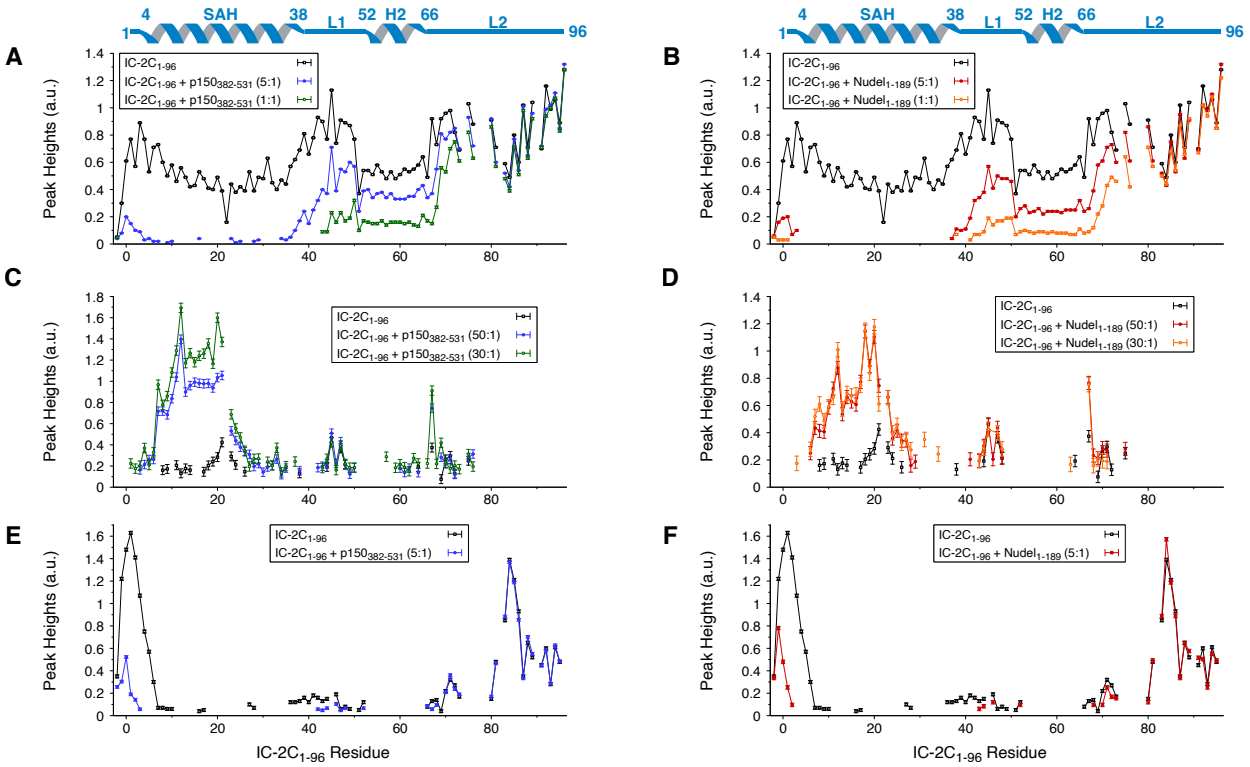

Figure 3. STD NMR and CLEANEX-PM experiments can be used to identify specific protein interfaces. (A,B) Relative peak heights for amide protons from ^{1}H-^{15}N HSQC-TROSY spectra for IC-2C$_{1\text{-}96}$ without a binding partner (black), with a substoichiometric amount of p150$_{382\text{-}531}$ (5:1, blue) or Nudel$_{1\text{-}189}$ (5:1, red), and with a stoichiometric amount of p150$_{382\text{-}531}$ (1:1, green) or Nudel$_{1\text{-}189}$ (1:1, orange) show that amide protons in the SAH region are greatly affected by binding and that amide protons from the H2 region are also affected. **(C,D)** TROSY-based STD NMR data for amide protons for IC-2C$_{1\text{-}96}$ without a binding partner (black), with a very low amount of p150$_{382\text{-}531}$ (50:1, blue) or Nudel$_{1\text{-}189}$ (50:1, red), and with slightly more p150$_{382\text{-}531}$ (30:1, green) or Nudel$_{1\text{-}189}$ (30:1, orange), show that residues 7-21 of IC-2C experience the most saturation transfer. **(E,F)** Relative peak heights from (CLEANEX-PM)-TROSY spectra with a 100 ms mixing time for IC-2C$_{1\text{-}96}$ without a binding partner (black) and with a substoichiometric amount of p150$_{382\text{-}531}$ (5:1, blue) or Nudel$_{1\text{-}189}$ (5:1, red), show that the N-terminal region of the SAH region becomes more protected upon binding, whereas the rates of exchange for the L2 region are unchanged. The error bars are based on root-mean-square noise in the spectra. All data were collected at 15ºC at 800 MHz for ^{1}H using a ^{2}H,^{15}N-labeled IC-2C$_{1\text{-}96}$ sample in 95% H_2O/5% D_2O. Residues –3 to 0 correspond to non-native residues (GAHM); residue 1 corresponds to the first native residue of IC-2C.

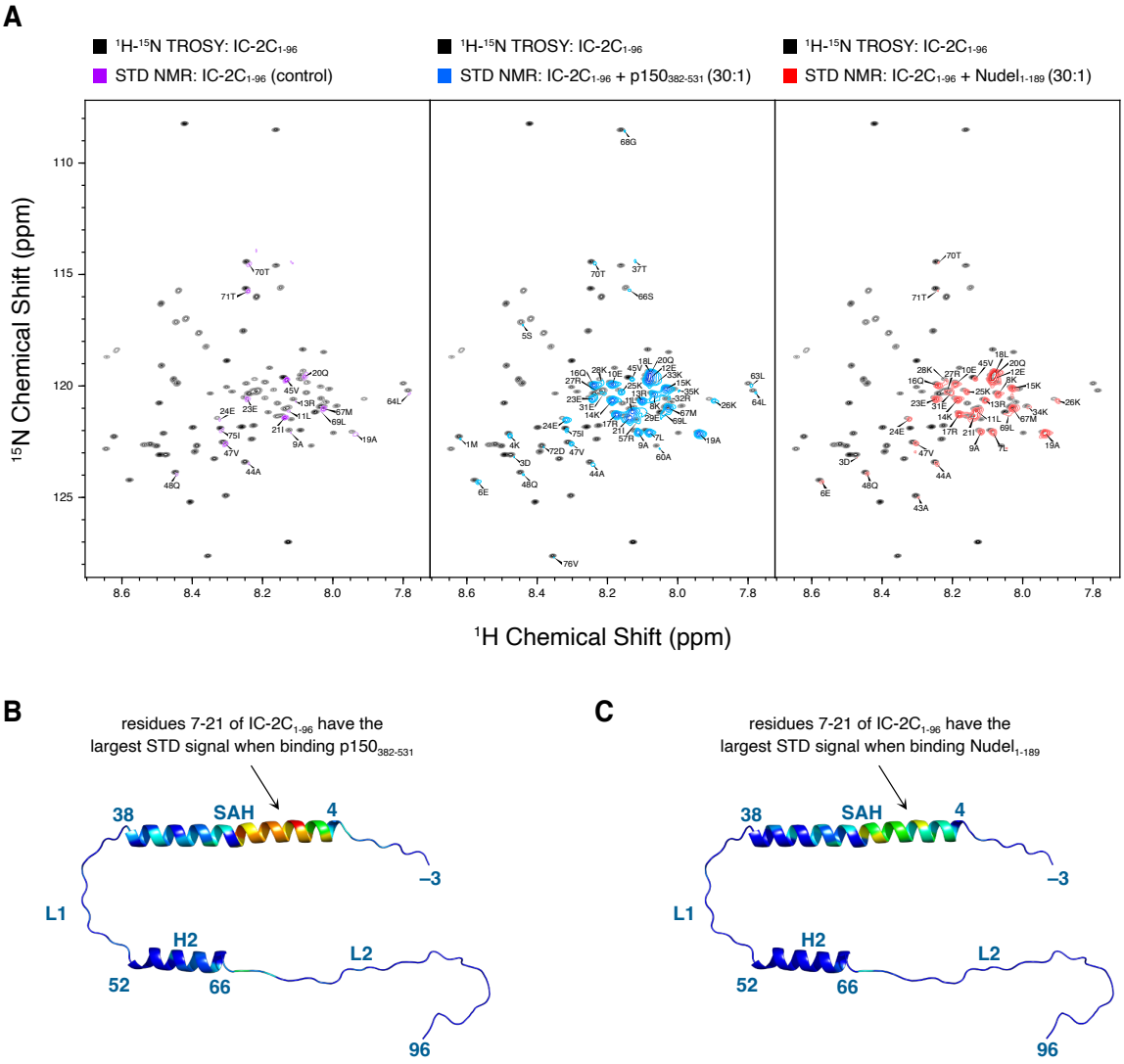

Figure 4. NMR spectra demonstrating how STD NMR unambiguously assigns the residues of IC-2C$_{1\text{-}96}$ that are involved in binding p150$_{382\text{-}531}$ and Nudel$_{1\text{-}189}$. (A) Shown are a ^{1}H-^{15}N HSQC-TROSY spectrum for IC-2C$_{1\text{-}96}$ (black) and STD NMR spectra for a control sample with just IC-2C$_{1\text{-}96}$ (purple, left), a substoichiometric amount of p150$_{382\text{-}531}$ (30:1, blue, center) or a substoichiometric amount of Nudel$_{1\text{-}189}$ (30:1, red, right). For clarity, the STD NMR spectra are offset by 0.01 ppm in the ^{1}H dimension and by 0.1 ppm in the ^{15}N dimension. All data were collected at 15ºC at 800 MHz for ^{1}H using a ^{2}H,^{15}N-labeled IC-2C$_{1\text{-}96}$ sample in 95% H_2O/5% D_2O. Residues –3 to 0 correspond to non-native residues (GAHM); residue 1 corresponds to the first native residue of IC-2C. **(B,C)** STD NMR results mapped onto a model of IC-2C$_{1\text{-}96}$ generated using PyMOL [48]. Values used are the difference between the STD signal when the binding partner [p150$_{382\text{-}531}$ **(B)** or Nudel$_{1\text{-}189}$ **(C)**] is present and the STD signal for the control sample. Red indicates the largest STD signals and dark blue indicates no effect; both models are colored using the same scale. The highest STD signal is observed for residues 7-21 of IC-2C$_{1\text{-}96}$ in both cases, indicating that p150$_{382\text{-}531}$ and Nudel$_{1\text{-}189}$ share the same binding site.

Discussion

The partially disordered dynein intermediate chain (IC) is central to dynein regulation and assembly as it binds dynein regulators dynactin p150^{Glued} and NudE/Nudel with α-helical regions at the N-terminus, three dynein light chains with intrinsically disordered regions in the middle, and the dynein heavy chain with the folded β-propeller domain at the C-terminus. Here, we focus on the p150^{Glued} and NudE/Nudel binding domain of IC, which contains the SAH region of approximately 35 residues and a shorter helix of approximately 10 residues (H2) that is separated from the SAH region by a disordered linker (L1). Our ongoing investigations are based on the hypothesis that although the SAH region is the major binding site for both p150^{Glued} and NudE/Nudel in all species studied (yeast, *Chaetomium thermophilum*, Drosophila, and mammalian), the H2 region underlies the selection of IC binding to p150^{Glued} and NudE/Nudel by a mechanism that is conserved among yeast, *Chaetomium*, and Drosophila but differs for mammalian IC, which has a more complex mechanism for the regulation of its binding interactions.

Among these four organisms the N-terminal region of IC varies in the level of secondary structure of the H2 region, in the length of the L1 linker region between the SAH and H2 regions, and by the degree to which the H2 region binds directly to p150^{Glued}. The H2 region forms a nascent helix in Drosophila, yeast, and *Chaetomium* IC but is fully folded in mammalian IC. In titration experiments that were followed by NMR spectroscopy, complete attenuation of peaks for all residues in the SAH region was observed in the NMR spectra, and considerable peak attenuation was observed for residues from the H2 region for ICs from all species. While peak attenuation is frequently interpreted as being due to binding, there are other possible reasons for peaks to disappear and therefore more experiments were conducted for determining whether the H2 region directly interacts with IC's binding partners.

Removal of the H2 region in Drosophila, yeast, and *Chaetomium* IC diminishes p150^{Glued} binding [6,33,35], while removal of this region from mammalian IC has no measurable effect on p150^{Glued} binding in isothermal titration calorimetry experiments [34]. In *Chaetomium* IC, a construct containing the H2 region but not the SAH region still binds to p150^{Glued}, thus explaining why the H2 region is necessary for tight binding [35]. Similarly, NMR titrations of Drosophila p150^{Glued} in a pre-formed NudE/IC binary complex show that p150^{Glued} can displace NudE but, in contrast, the reciprocal experiment involving an excess of NudE does not show displacement of p150^{Glued} [13,62]. We attributed these differences to the involvement of the H2 region in p150^{Glued} binding, as some conformations of the NudE/IC ensemble will expose the H2 region, leaving it accessible to p150^{Glued}. Consequently, mass action in a mixture of NudE and p150^{Glued} with IC will result in the p150^{Glued}/IC complex becoming more highly populated.

The question we ask here is whether the H2 region in mammalian IC interacts directly with p150^{Glued} or whether there are other reasons for the selection of p150^{Glued} over Nudel. We show that in the IC-2C$_{1\text{-}96}$ construct there is a significant PRE in either H2 or SAH when the MTSL label was located in the SAH (A9C) or H2 (A62C) regions, respectively (Figure 1A). From this, we infer that H2 has transient interactions with residues 14–29 of the SAH, as shown in the model in Figure 1C. In addition, with the MTSL label located in the intrinsically disordered L2 region (A93C), a very small increase in the PRE values in the middle of the SAH region was observed, indicating a low-frequency, transient interaction between those parts of IC-2C. A transient structure in this region has not been previously observed based on secondary chemical shifts or

relaxation measurements [34], demonstrating the power of PRE measurements to probe transient interactions.

To determine whether H2 binds directly to $p150^{Glued}$, we used STD NMR to identify amide protons of IC that are in direct contact with $p150^{Glued}$. STD NMR saturates methyl protons of the binding partner, which will only transfer signal to amides with which they are in direct contact. An increase in the STD signal for amides in the SAH region of $IC\text{-}2C_{1\text{-}96}$ confirmed that this region of IC-2C binds to $p150^{Glued}$ and allowed the identification of residues 7-21 as the most affected (Figure 3C), while the absence of a change in the STD signal for residues in the H2 region clearly indicated that there is no direct interaction with $p150^{Glued}$, and therefore that the peak attenuation observed for this region upon binding $p150^{Glued}$ is due to a relayed effect caused by the packing of the H2 region against the SAH region.

Amide hydrogen exchange is another powerful method for identifying transient structures, to determine helix stability, and for mapping binding sites. Most significantly here, CLEANEX experiments show that the most stable part of the SAH region begins at residue 7 rather than, as previously predicted from secondary chemical shifts, residue 4, and that residues 1-6 of the SAH region become significantly stabilized upon binding with both $p150^{Glued}$ and Nudel (Figures 3E and 3F). It is interesting to note that the serine-rich region is considerably more labile than the disordered residues flanking it, and this solvent exposure is not affected by $p150^{Glued}$ and Nudel binding. This observation helps confirm that the $p150^{Glued}$/Nudel binding region of IC is distant from the phosphorylation sites and that the exposure of the phosphorylation sites to kinases remains the same between the free and bound states.

Taken together, the lack of direct engagement of the mammalian H2 region in driving selective binding to $p150^{Glued}$ and Nudel appears to be a property of mammalian IC. In the absence of the involvement of the H2 region in binding we do not believe that there is a similar pathway for competitive binding between $p150^{Glued}$ and Nudel with IC in mammalian systems in the way that we have proposed for Drosophila IC. These results not only have a far-reaching impact on our understanding of processes essential for dynein regulation, but also offer a novel role for protein disorder in controlling cellular processes and highlight the advantages of NMR spectroscopy in elucidating atomic-level characterization of extremely complex dynamic cellular assemblies.

Perspective

Solid-state NMR and cryo-electron microscopy have significantly advanced the size and resolution capabilities for studying large protein complexes. Cryo-electron microscopy, in particular, offers the advantage of requiring only small quantities of proteins under native or near-native conditions. Additionally, AlphaFold and its updated versions have made modeling large proteins and protein complexes more feasible. However, these methods fall short when it comes to identifying transient structures within IDPs or transient binding interfaces within IDP complexes. Currently, only solution-state NMR can provide detailed information about dynamic structures and interfaces, despite the challenges associated with producing and analyzing these proteins and complexes. The NMR techniques presented in our study are practical and can be seamlessly integrated into the analysis of proteins for which production methods and resonance assignments are already established.

Acknowledgements

We acknowledge support from the National Science Foundation (Award 1617019 for E.J.B. and Award 2003557 for N.M.L.). The 800 MHz NMR spectrometer at the Oregon State University NMR Facility was funded in part by the National Institutes of Health (HEI Grant 1S10OD018518) and by the M. J. Murdock Charitable Trust (Grant 2014162).

References

[1] E. Barbar, A. Nyarko, Polybivalency and disordered proteins in ordering macromolecular assemblies, Semin. Cell Dev. Biol. 37 (2015) 20–25. https://doi.org/10.1016/j.semcdb.2014.09.016.

[2] R.B. Berlow, H.J. Dyson, P.E. Wright, Expanding the paradigm: intrinsically disordered proteins and allosteric regulation, J. Mol. Biol. 430 (2018) 2309–2320. https://doi.org/10.1016/j.jmb.2018.04.003.

[3] V. Csizmok, J.D. Forman-Kay, Complex regulatory mechanisms mediated by the interplay of multiple post-translational modifications, Curr. Opin. Struct. Biol. 48 (2018) 58–67. https://doi.org/10.1016/j.sbi.2017.10.013.

[4] S.L. Reck-Peterson, W.B. Redwine, R.D. Vale, A.P. Carter, The cytoplasmic dynein transport machinery and its many cargoes, Nat. Rev. Mol. Cell Biol. 19 (2018) 382–398. https://doi.org/10.1038/s41580-018-0004-3.

[5] M. Makokha, M. Hare, M. Li, T. Hays, E. Barbar, Interactions of cytoplasmic dynein light chains Tctex-1 and LC8 with the intermediate chain IC74, Biochemistry 41 (2002) 4302–4311. https://doi.org/10.1021/bi011970h.

[6] J.L. Morgan, Y. Song, E. Barbar, Structural dynamics and multiregion interactions in dynein-dynactin recognition, J. Biol. Chem. 286 (2011) 39349–39359. https://doi.org/10.1074/jbc.M111.296277.

[7] K.A. Jara, N.M. Loening, P.N. Reardon, Z. Yu, P. Woonnimani, C. Brooks, C.H. Vesely, E.J. Barbar, Multivalency, autoinhibition, and protein disorder in the regulation of interactions of dynein intermediate chain with dynactin and the nuclear distribution protein, eLife 11 (2022) e80217. https://doi.org/10.7554/eLife.80217.

[8] D.I. Nurminsky, M.V. Nurminskaya, E.V. Benevolenskaya, Y.Y. Shevelyov, D.L. Hartl, V.A. Gvozdev, Cytoplasmic dynein intermediate-chain isoforms with different targeting properties created by tissue-specific alternative splicing, Mol. Cell. Biol. 18 (1998) 6816–6825. https://doi.org/10.1128/mcb.18.11.6816.

[9] J. Ha, K.W.-H. Lo, K.R. Myers, T.M. Carr, M.K. Humsi, B.A. Rasoul, R.A. Segal, K.K. Pfister, A neuron-specific cytoplasmic dynein isoform preferentially transports TrkB signaling endosomes, J. Cell Biol. 181 (2008) 1027–1039. https://doi.org/10.1083/jcb.200803150.

[10] J. Whyte, J.R. Bader, S.B.F. Tauhata, M. Raycroft, J. Hornick, K.K. Pfister, W.S. Lane, G.K. Chan, E.H. Hinchcliffe, P.S. Vaughan, K.T. Vaughan, Phosphorylation regulates targeting of cytoplasmic dynein to kinetochores during mitosis, J. Cell Biol. 183 (2008) 819–834. https://doi.org/10.1083/jcb.200804114.

[11] V. van Dis, M. Kuijpers, E.D. Haasdijk, E. Teuling, S.A. Oakes, C.C. Hoogenraad, D. Jaarsma, Golgi fragmentation precedes neuromuscular denervation and is associated with endosome abnormalities in SOD1-ALS mouse motor neurons, Acta Neuropathol. Commun. 2 (2014) 38. https://doi.org/10.1186/2051-5960-2-38.

[12] N.J. Bradshaw, M.A.F. Hayashi, NDE1 and NDEL1 from genes to (mal)functions: parallel but distinct roles impacting on neurodevelopmental disorders and psychiatric illness, Cell. Mol. Life Sci. CMLS 74 (2016) 1191–1210. https://doi.org/10.1007/s00018-016-2395-7.
[13] A. Nyarko, Y. Song, E. Barbar, Intrinsic disorder in dynein intermediate chain modulates its interactions with NudE and dynactin, J. Biol. Chem. 287 (2012) 24884–24893. https://doi.org/10.1074/jbc.M112.376038.
[14] L. Urnavicius, K. Zhang, A.G. Diamant, C. Motz, M.A. Schlager, M. Yu, N.A. Patel, C.V. Robinson, A.P. Carter, The structure of the dynactin complex and its interaction with dynein, Science 347 (2015) 1441–1446. https://doi.org/10.1126/science.aaa4080.
[15] S.R. Garrott, M.E. DeSantis, CryoEM shows the active dynein complex on microtubules, Trends Biochem. Sci. 48 (2023) 315–316. https://doi.org/10.1016/j.tibs.2023.01.007.
[16] K. Singh, C.K. Lau, G. Manigrasso, J.B. Gama, R. Gassmann, A.P. Carter, Molecular mechanism of dynein-dynactin complex assembly by LIS1, Science 383 (2024) eadk8544. https://doi.org/10.1126/science.adk8544.
[17] B. Brutscher, I.C. Felli, S. Gil-Caballero, T. Hošek, R. Kümmerle, A. Piai, R. Pierattelli, Z. Sólyom, NMR methods for the study of instrinsically disordered proteins structure, dynamics, and interactions: general overview and practical guidelines, Adv. Exp. Med. Biol. 870 (2015) 49–122. https://doi.org/10.1007/978-3-319-20164-1_3.
[18] H.J. Dyson, P.E. Wright, NMR illuminates intrinsic disorder, Curr. Opin. Struct. Biol. 70 (2021) 44–52. https://doi.org/10.1016/j.sbi.2021.03.015.
[19] M. Schiavina, L. Bracaglia, T. Bolognesi, M.A. Rodella, G. Tagliaferro, A.S. Tino, R. Pierattelli, I.C. Felli, Intrinsically disordered proteins studied by NMR spectroscopy, J. Magn. Reson. Open 18 (2024) 100143. https://doi.org/10.1016/j.jmro.2023.100143.
[20] M.D. Mukrasch, S. Bibow, J. Korukottu, S. Jeganathan, J. Biernat, C. Griesinger, E. Mandelkow, M. Zweckstetter, Structural polymorphism of 441-residue tau at single residue resolution, PLoS Biol. 7 (2009) e1000034. https://doi.org/10.1371/journal.pbio.1000034.
[21] A. Nyarko, Y. Song, J. Nováček, L. Žídek, E. Barbar, Multiple recognition motifs in nucleoporin Nup159 provide a stable and rigid Nup159-Dyn2 assembly, J. Biol. Chem. 288 (2013) 2614–2622. https://doi.org/10.1074/jbc.M112.432831.
[22] S. Clark, J.B. Myers, A. King, R. Fiala, J. Novacek, G. Pearce, J. Heierhorst, S.L. Reichow, E.J. Barbar, Multivalency regulates activity in an intrinsically disordered transcription factor, eLife 7 (2018) e36258. https://doi.org/10.7554/eLife.36258.
[23] A.S. Krois, H.J. Dyson, P.E. Wright, Long-range regulation of p53 DNA binding by its intrinsically disordered N-terminal transactivation domain, Proc. Natl. Acad. Sci. U. S. A. 115 (2018) E11302–E11310. https://doi.org/10.1073/pnas.1814051115.
[24] N.E. Jespersen, C. Leyrat, F.C. Gérard, J.-M. Bourhis, D. Blondel, M. Jamin, E. Barbar, The LC8-RavP ensemble structure evinces a role for LC8 in regulating Lyssavirus polymerase functionality, J. Mol. Biol. 431 (2019) 4959–4977. https://doi.org/10.1016/j.jmb.2019.10.011.
[25] M.A. Lietzow, M. Jamin, H.J. Dyson, P.E. Wright, Mapping long-range contacts in a highly unfolded protein, J. Mol. Biol. 322 (2002) 655–662. https://doi.org/10.1016/s0022-2836(02)00847-1.
[26] G.M. Clore, J. Iwahara, Theory, practice, and applications of paramagnetic relaxation enhancement for the characterization of transient low-population states of biological macromolecules and their complexes, Chem. Rev. 109 (2009) 4108–4139. https://doi.org/10.1021/cr900033p.

[27] S. Clark, A. Nyarko, F. Löhr, P.A. Karplus, E. Barbar, The anchored flexibility model in LC8 motif recognition: insights from the chica complex, Biochemistry 55 (2016) 199–209. https://doi.org/10.1021/acs.biochem.5b01099.
[28] M. Mayer, B. Meyer, Characterization of ligand binding by saturation transfer difference NMR spectroscopy, Angew. Chem. Int. Ed Engl. 38 (1999) 1784–1788. https://doi.org/10.1002/(SICI)1521-3773(19990614)38:12<1784::AID-ANIE1784>3.0.CO;2-Q.
[29] B. Meyer, T. Peters, NMR spectroscopy techniques for screening and identifying ligand binding to protein receptors, Angew. Chem. Int. Ed Engl. 42 (2003) 864–890. https://doi.org/10.1002/anie.200390233.
[30] C.E. Dempsey, Hydrogen exchange in peptides and proteins using NMR spectroscopy, Prog. Nucl. Magn. Reson. Spectrosc. 39 (2001) 135–170. https://doi.org/10.1016/S0079-6565(01)00032-2.
[31] D. Long, G. Bouvignies, L.E. Kay, Measuring hydrogen exchange rates in invisible protein excited states, Proc. Natl. Acad. Sci. 111 (2014) 8820–8825. https://doi.org/10.1073/pnas.1405011111.
[32] A.E. Siglin, S. Sun, J.K. Moore, S. Tan, M. Poenie, J.D. Lear, T. Polenova, J.A. Cooper, J.C. Williams, Dynein and dynactin leverage their bivalent character to form a high-affinity interaction, PloS One 8 (2013) e59453. https://doi.org/10.1371/journal.pone.0059453.
[33] J. Jie, F. Löhr, E. Barbar, Interactions of yeast dynein with dynein light chain and dynactin: general implications for intrinsically disordered duplex scaffolds in multiprotein assemblies, J. Biol. Chem. 290 (2015) 23863–23874. https://doi.org/10.1074/jbc.M115.649715.
[34] J. Jie, F. Löhr, E. Barbar, Dynein Binding of Competitive Regulators Dynactin and NudE Involves Novel Interplay between Phosphorylation Site and Disordered Spliced Linkers, Structure 25 (2017) 421–433. https://doi.org/10.1016/j.str.2017.01.003.
[35] N.M. Loening, S. Saravanan, N.E. Jespersen, K. Jara, E. Barbar, Interplay of disorder and sequence specificity in the formation of stable dynein-dynactin complexes, Biophys. J. 119 (2020) 950–965. https://doi.org/10.1016/j.bpj.2020.07.023.
[36] M. Jansson, Y.C. Li, L. Jendeberg, S. Anderson, G.T. Montelione, B. Nilsson, High-level production of uniformly ^{15}N- and ^{13}C-enriched fusion proteins in *Escherichia coli*, J. Biomol. NMR 7 (1996) 131–141.
[37] S.M. Davis, B.L. Romig, A.A. Abe, N.M. Loening, An improved variant of tobacco etch virus (TEV) protease that does not need reducing agents, Protein Sci. Publ. Protein Soc. 34 (2025) e70049. https://doi.org/10.1002/pro.70049.
[38] V. Venditti, N.L. Fawzi, Probing the atomic structure of transient protein contacts by paramagnetic relaxation enhancement solution NMR, Methods Mol. Biol. Clifton NJ 1688 (2018) 243–255. https://doi.org/10.1007/978-1-4939-7386-6_12.
[39] A. Di Nicola, B.L. Romig, S.M. Davis, P.H. Cleary, C.H. Yung, D.R. Marsan, A.C. Merkt, N.M. Loening, Investigating binding between dynein intermediate chain and dynactin p150^{Glued}, Protein Sci. Publ. Protein Soc. TBD (2025).
[40] Z. Solyom, M. Schwarten, L. Geist, R. Konrat, D. Willbold, B. Brutscher, BEST-TROSY experiments for time-efficient sequential resonance assignment of large disordered proteins, J. Biomol. NMR 55 (2013) 311–321. https://doi.org/10.1007/s10858-013-9715-0.
[41] L.W. Donaldson, N.R. Skrynnikov, W.Y. Choy, D.R. Muhandiram, B. Sarkar, J.D. Forman-Kay, L.E. Kay, Structural characterization of proteins with an attached ATCUN motif by

paramagnetic relaxation enhancement NMR spectroscopy, J. Am. Chem. Soc. 123 (2001) 9843–9847. https://doi.org/10.1021/ja011241p.

[42] W.F. Vranken, W. Boucher, T.J. Stevens, R.H. Fogh, A. Pajon, M. Llinas, E.L. Ulrich, J.L. Markley, J. Ionides, E.D. Laue, The CCPN data model for NMR spectroscopy: development of a software pipeline, Proteins 59 (2005) 687–696. https://doi.org/10.1002/prot.20449.

[43] N. Bloembergen, L.O. Morgan, Proton relaxation times in paramagnetic solutions. Effects of electron spin relaxation, J. Chem. Phys. 34 (1961) 842–850. https://doi.org/10.1063/1.1731684.

[44] P.A. Kosen, Spin labeling of proteins, in: Methods Enzymol., Academic Press, 1989: pp. 86–121. https://doi.org/10.1016/0076-6879(89)77007-5.

[45] J. Iwahara, C.D. Schwieters, G.M. Clore, Ensemble approach for NMR structure refinement against ^{1}H paramagnetic relaxation enhancement data arising from a flexible paramagnetic group attached to a macromolecule, J. Am. Chem. Soc. 126 (2004) 5879–5896. https://doi.org/10.1021/ja031580d.

[46] L. Salmon, G. Nodet, V. Ozenne, G. Yin, M.R. Jensen, M. Zweckstetter, M. Blackledge, NMR characterization of long-range order in intrinsically disordered proteins, J. Am. Chem. Soc. 132 (2010) 8407–8418. https://doi.org/10.1021/ja101645g.

[47] P.S. Vaughan, J.D. Leszyk, K.T. Vaughan, Cytoplasmic dynein intermediate chain phosphorylation regulates binding to dynactin, J. Biol. Chem. 276 (2001) 26171–26179. https://doi.org/10.1074/jbc.M102649200.

[48] The PyMOL molecular graphics system, version 3.0, (n.d.).

[49] T.-L. Hwang, S. Mori, A.J. Shaka, P.C.M. van Zijl, Application of phase-modulated CLEAN chemical EXchange spectroscopy (CLEANEX-PM) to detect water−protein proton exchange and intermolecular NOEs, J. Am. Chem. Soc. 119 (1997) 6203–6204. https://doi.org/10.1021/ja970160j.

[50] G. Hernández, D.M. LeMaster, Relaxation compensation in chemical exchange measurements for the quantitation of amide hydrogen exchange in larger proteins, Magn. Reson. Chem. 41 (2003) 699–702. https://doi.org/10.1002/mrc.1239.

[51] R. Li, C. Woodward, The hydrogen exchange core and protein folding, Protein Sci. Publ. Protein Soc. 8 (1999) 1571–1590. https://doi.org/10.1110/ps.8.8.1571.

[52] K. Pervushin, R. Riek, G. Wider, K. Wüthrich, Attenuated T_2 relaxation by mutual cancellation of dipole–dipole coupling and chemical shift anisotropy indicates an avenue to NMR structures of very large biological macromolecules in solution, Proc. Natl. Acad. Sci. 94 (1997) 12366–12371. https://doi.org/10.1073/pnas.94.23.12366.

[53] R.A. Venters, C.-C. Huang, B.T. Farmer, R. Trolard, L.D. Spicer, C.A. Fierke, High-level ^{2}H/^{13}C/^{15}N labeling of proteins for NMR studies, J. Biomol. NMR 5 (1995) 339–344. https://doi.org/10.1007/BF00182275.

[54] M. Sattler, S.W. Fesik, Use of deuterium labeling in NMR: overcoming a sizeable problem, Structure 4 (1996) 1245–1249. https://doi.org/10.1016/S0969-2126(96)00133-5.

[55] S. Schütz, R. Sprangers, Methyl TROSY spectroscopy: A versatile NMR approach to study challenging biological systems, Prog. Nucl. Magn. Reson. Spectrosc. 116 (2020) 56–84. https://doi.org/10.1016/j.pnmrs.2019.09.004.

[56] J.L. Morgan, A. Yeager, A.B. Estelle, J. Gsponer, E. Barbar, Transient tertiary structures of disordered dynein intermediate chain regulate its interactions with multiple partners, J. Mol. Biol. 433 (2021) 167152. https://doi.org/10.1016/j.jmb.2021.167152.

[57] J.P. MacKay, G.L. Shaw, G.F. King, Backbone dynamics of the c-Jun leucine zipper: ^{15}N NMR relaxation studies, Biochemistry 35 (1996) 4867–4877. https://doi.org/10.1021/bi952761y.
[58] N.M. Loening, E. Barbar, Structural characterization of the self-association domain of swallow, Protein Sci. Publ. Protein Soc. 30 (2021) 1056–1063. https://doi.org/10.1002/pro.4055.
[59] R.B. Vallee, R.J. McKenney, K.M. Ori-McKenney, Multiple modes of cytoplasmic dynein regulation, Nat. Cell Biol. 14 (2012) 224–230. https://doi.org/10.1038/ncb2420.
[60] V.P. Efimov, N.R. Morris, The LIS1-related NUDF protein of *Aspergillus nidulans* interacts with the coiled-coil domain of the NUDE/RO11 protein, J. Cell Biol. 150 (2000) 681–688. https://doi.org/10.1083/jcb.150.3.681.
[61] R.J. McKenney, S.J. Weil, J. Scherer, R.B. Vallee, Mutually exclusive cytoplasmic dynein regulation by NudE-Lis1 and dynactin, J. Biol. Chem. 286 (2011) 39615–39622. https://doi.org/10.1074/jbc.M111.289017.
[62] E. Barbar, Native disorder mediates binding of dynein to NudE and Dynactin, Biochem. Soc. Trans. 40 (2012) 1009–1013. https://doi.org/10.1042/BST20120180.